Application of machine learning and resistivity measurements for 3D apparent geological modeling in the Yilan plain, Taiwan, at the SW Tip of the Okinawa trough

Ping-Yu Chang[1,2,3]* , Jordi Mahardika Puntu[1], Ding-Jiun Lin[1], Haiyina Hasbia Amania[1], Wen-Shan Chen[4] and Andrew Tien-shun Lin[1]

Abstract

This study presents a pioneering investigation into the complex Holocene paleo-morphologies of the Yilan Plain, located at the southwestern edge of the Okinawa Trough. We employed a novel approach that synergized resistivity measurements with machine learning techniques to unlock valuable insights into the geological history, sedimentary patterns, and seismic activity of this dynamic region. Our methodology involved the creation of an Apparent Geological Model (AGM) through the interpolation of inverted resistivity data and the application of supervised machine learning algorithms. Classification criteria, derived from the relationship between resistivity values and sediment types found in nearby boreholes, were developed using the random forest machine-learning method. The resultant 3D resistivity model was transformed into a clay-sand-gravel model, offering a comprehensive depiction of sediment distribution within the Yilan Plain. Notably, our findings revealed distinct sedimentary patterns. Gravel-dominated regions, characterized by resistivity values above 140 Ohm-m, were identified alongside areas dominated by sand and clay sediments. The Carbon-14 dating ages in the sand sediments exhibited remarkable consistency, shedding light on the depositional history of the region. Furthermore, our research unveiled a previously unknown phenomenon of rapid subsidence in the Yilan Plain. Through meticulous analysis and correction for sea-level changes, we estimated an average subsidence rate of approximately 8.5 mm/year. This subsidence was punctuated by abrupt events around 6000–7000 years BP and 2000–3000 years BP, associated with a sudden increase. These events suggested a potential link to prehistoric seismic activity, with variable subsidence rates between episodes hinting at recurrent active seismic periods every 4000–5000 years. In conclusion, our multidisciplinary approach has provided unprecedented insights into the Holocene paleo-morphologies of the Yilan Plain. By combining resistivity measurements, machine learning, and geological analysis, we have enriched our understanding of the region's geological history, sedimentary dynamics, and seismic behavior. These findings not only contribute to the knowledge of Yilan's past but also offer vital data for future environmental and geological studies in similarly dynamic regions.

*Correspondence:
Ping-Yu Chang
pingyuc@ncu.edu.tw
Full list of author information is available at the end of the article

Chang *et al. Geoscience Letters*   (2024) 11:25

Page 2 of 15

Key Points

- The study investigates Holocene paleo-morphologies in Taiwan's Yilan Plain, providing insights into its geological history.
- By combining resistivity measurements with machine learning, the research unveils valuable data on sedimentary patterns and seismic activity in the region.
- The methodology includes creating an Apparent Geological Model (AGM) using machine learning algorithms and resistivity data interpolation.
- The study establishes classification criteria and models sediment distribution, identifying distinct patterns in clay, sand, and gravel.
- The research reveals rapid subsidence and suggests links to prehistoric seismic events with a 4000-5000 recurrence period.

Keywords Apparent Geological Model (AGM), Resistivity measurements, Machine learning, Okinawa Trough

Introduction

In the study we attempted to use both the resistivity measurements and the core records for reconstructing the 3D geological model via machine learning to analyze the evolution of Holocene paleo-morphologies of the Yilan plain in the northeastern Taiwan. The plain is located on the southwest tip of the Okinawa Trough (Fig. 1). Since the Okinawa Trough is thought to be the back-arc opening related to the convergence of the Philippine Sea Plate and the Eurasian Plate, the Yilan Plain is considered crucial for understanding the recent back-arc opening mode of the Okinawa Trough. Researchers usually rely on the wellbore logs and core samples to determine the subsurface stratigraphy of unconsolidated Holocene sediments [*Izquierdo*, 2014]. Marine seismic explorations have shown that the extension of the Okinawa Trough has undergone two phases: the Pleistocene phase from 2 to 0.1 million years ago, and the recent phase from 0.1 million years ago to the present (Sibuet et al. 1998). And that extension in the last phase involves activities of nearly EW-trending normal faults dipping toward the Okinawa Trough axis with offsets ranging in length from a few meters to tens of meters (Lai et al. 2009; Sibuet et al. 1998) in the westernmost part of the trough off the Yilan Plain. From their on-land seismic explorations in the Yilan Plain, Chiang (1976) showed that there are also mainly EW-trending faults dipping south in the Yilan Plain. Chang et al. (2020) found that the Yilan area features a series of N-S trending fracture zones in addition to the normal fault systems from the results of the AMT, deep borehole logs, and reinterpreted seismic surveys. However, the amount of accountable wellbore logs is few because of their high costs and time consuming in drilling wells [*Wojda and Brouyère*, 2013]. Therefore, geologists usually construct the fence diagrams or the conceptual geological models, which show rough trends of the geological structures in the subsurface from limited number of wellbore logs, to describe the stratigraphy of unconsolidated sediments in regional scale. Unfortunately, these models may miss the local heterogeneity, for instance, the local coarse-grain river channels or oxbow lake deposits because there are usually few wellbore data accessible in the area. As a result, one may have very different explanations for the conceptual model due to the insufficient well logs and the subjective judgment in the correlation processes.

In recent years, researchers (i.e.,Beresnev et al. 2002; Bersezio et al. 2007; Rucker et al. 2011) applied surface electrical resistivity to facilitate the identification of sediment structure for a local area. The interpretation of acquired electrical resistivity data were made based on the resistivity range of different sediment types in some researches (i.e., Pellicer & Gibson 2011). To integrate the resistivity measurements and the wellbore data, we first interpolated the inverted resistivity data with inverse distance method to construct the 3D model. Then we developed the classification criteria based on the relationships of resistivity values and the registered sediment types in the nearby boreholes with the supervised machine-learning optimization method. Then we Lastly, we applied the aforementioned classification criteria to transform the model of resistivities into sediment types in order to delineate the three-dimensional stratigraphy of unconsolidated sediments (i.e. the apparent geological model, AGM). The derived high-resolution AGM model can be used for further analyze the depositional environment in our study area and compare the estimated sedimentary features with the history of environmental evolution.

Chang *et al. Geoscience Letters* (2024) 11:25

Page 3 of 15
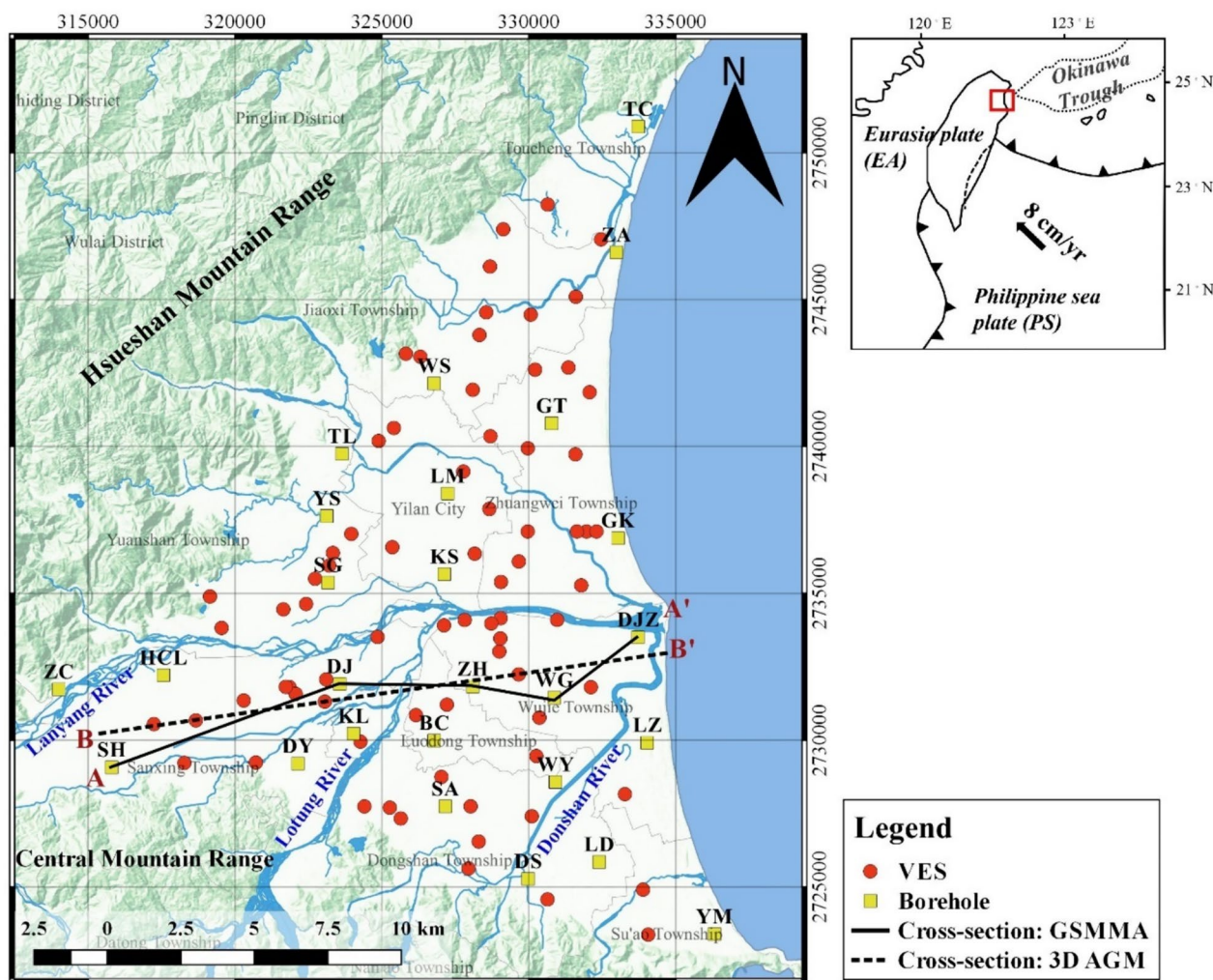
Fig. 1 The Yilan plain is located in northeastern Taiwan and on the southwestern tip of the Okinawa Trough. Red circles and yellow squares show the locations of Vertical Electrical Sounding (VES) measurements and the Borehole Records data from the observation wells, respectively. The AA' and BB' depicted the cross-section profiles from GSMMA and 3D AGM (This study)

Geological setting of the study area

The Yilan Plain is located in northeastern Taiwan and is thought to be an extension of the Okinawa Trough within the Eurasian continental lithosphere (Lai et al. 2009). The recent extension of the Okinawa Trough started approximately 0.1 million years ago. This extension movement involved ENE- and WSW-trending normal faults that dip toward the axis of the Okinawa Trough, with offsets ranging from a few meters to tens of meters (Lai et al. 2009; Sibuet et al. 1998).

The triangular plain is geographically bounded by the Hsueshan Mountain Range to the north, the Central Mountain Range to the south, and the Pacific Ocean to the east. Unconsolidated alluvial deposits from the Lanyang River and Lotung River were laid over the Paleogene rock basement, exhibiting normal faults(Chiang 1976; Hsu et al. 1996), identified from seismic reflection and refraction profiles. Figure 2 shows the borehole logs, carbon-14 dating records, and interpretations of the sedimentary environments of selected boreholes from the upper fan to the lower fan in Yilan (W. S. Chen 2000; GSMMA 2001a, b). In general, the upper fan mainly consists of gravel, and sediments gradually transition into clay-dominated ones towards the lower fan. In addition, young sediment has been deposited on the plain at an extremely high deposition rate, exceeding a thickness of 20 m within the last 3,000 years, as indicated by wellbore drilling data. Consequently, the thickness of the unconsolidated deposits can range from 100 m to over 800 m thick in the Yilan plain. These findings imply that the plain has undergone rapid subsidence recently.
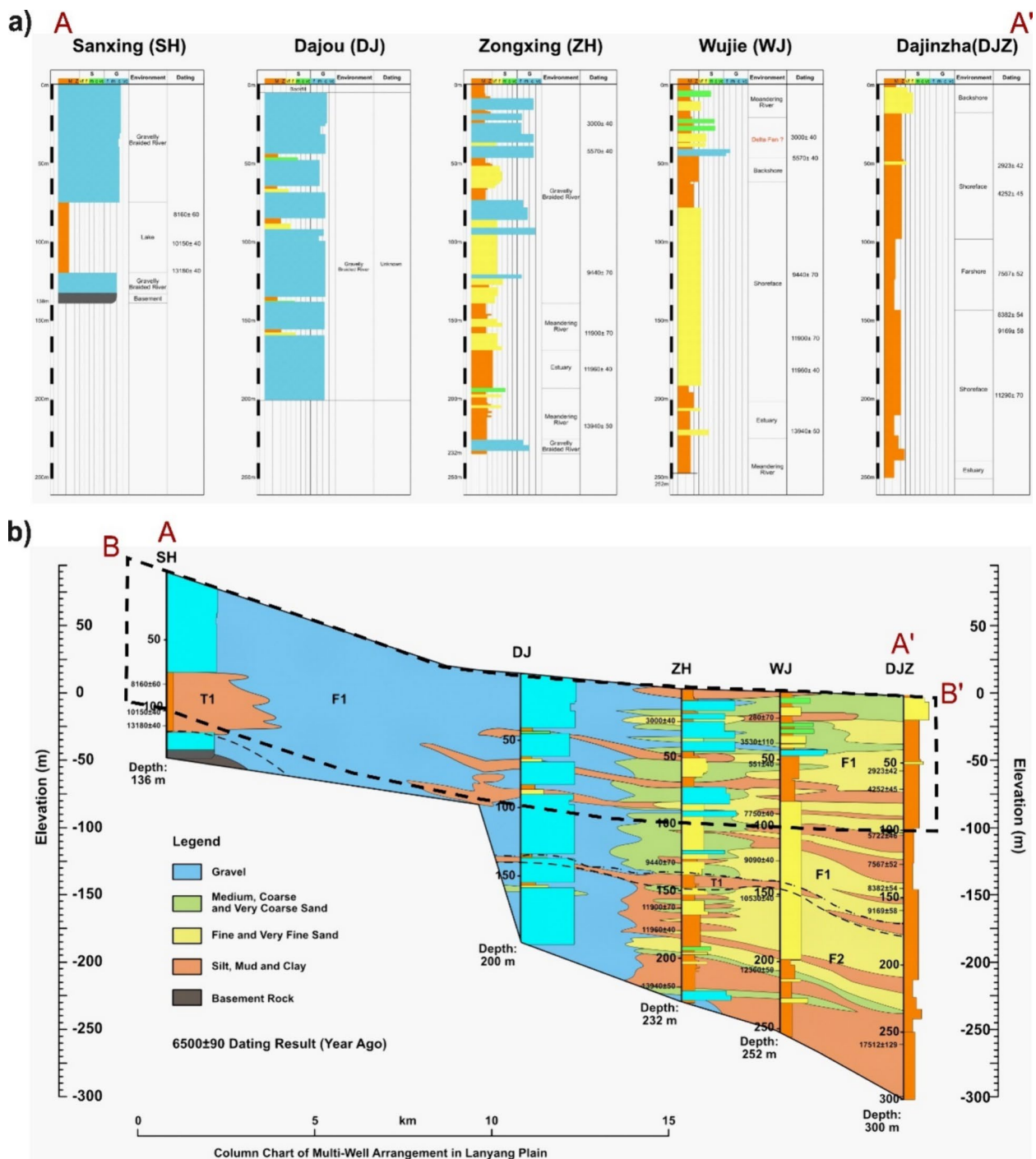
Fig. 2 a Selected borehole logs, sedimentary environments, and dating records of the AA' profile in Fig. 1 (W. S. Chen 2000; GSMMA 2001a, b; GSMMA 2001a, b). Borehole logs are resampled and modified from (GSMMA 2001a, b). The blue color represents gravels, yellow color shows sand, and orange color represents clays. **b** The Cross-section of AA' profile after GSMMA (2023). The dashed black box (BB' profile) depicts the cross-sectional view derived from the 3D AGM

Three major factors could affect the changes in Holocene coastal plain morphologies, including sea-level changes, sedimentation rates, and basin subsidence in the Yilan plain. In most low-lying areas around the world, rapid sea-level rise in the early Holocene dominated the evolution of coastal environments (Amato et al. 2013;

Chang *et al. Geoscience Letters*   (2024) 11:25

Page 5 of 15

Stanley & Warne 1994). After the sea level stabilized during the mid- to late Holocene, propagation and neo-tectonics became the major factors controlling changes in the coastal environment (Antonioli et al. 2009; Bird et al. 2010; Li et al. 2014). The interaction between these factors resulted in the complicated morphologies of the coastal environment in the Yilan plain. To reconstruct the paleomorphology, it is necessary to use non-destructive, high-resolution geophysical methods to better resolve the subsurface structure of sediment imaging.

The resistivity measurements and wellbore data

The data used in the study include 75 surface resistivity surveys, and 30 wellbore logs from different depths of the groundwater monitoring wells maintained by Taiwan's Water Resource Agency. 57 of the resistivity measurements were one-dimensional (1D) Vertical Electrical Sounding Surveys (VES) collected by Taiwan's Geological Survey and Mining Management Agency (GSMMA 2001a, b) with the Schlumberger arrays. The half-spacing between the two current electrodes (AB/2) was increased from 8-m to 800-m. And the half-spacing of the potential electrodes (MN/2) was 3-m, 30-m for AB/2 larger than 80-m, and 200-m for AB/2 larger than 200-m. The original VES measurements are apparent resistivity and are inverted individually to provide the 1D vertical resistivity

model at each survey location. This inversion process utilized an open-source Python package named *SimPEG* (Simulation and Parameter Estimation in Geophysics). For a comprehensive understanding of the inversion procedure, we forward readers to Cockett et al. (2015). Originally, the 1D inverted VES result extended to a depth of 250 m. However, considering the decrease in resolution of the VES with increasing depth, we limited the utilization of the inversion result to depths up to 100 m. In addition, we collected two dimensional (2D) electrical resistivity imaging (ERI) surveys at 14 locations with Wenner-Schlumberger arrays recently. The electrode spacing is 10-m and the maximum length of the survey line is 330-m in the ERI surveys. The 2D data are inverted with the EarthImager2D™ code for construct the 2D resistivity profile. We then extract the selected 1D resistivity column from the profile for representing the vertical resistivity change at the survey site. All the resistivity measurements were then combined and will be used for constructing the regional 3D resistivity model with the inverse distance interpolation methods.

To see the relationships between the resistivity and the sediments, we compared the resistivity measured near the boreholes to the predominant sediment types recorded at the same depth range in the borehole logs. The wellbore logs were registered in 10-cm intervals and
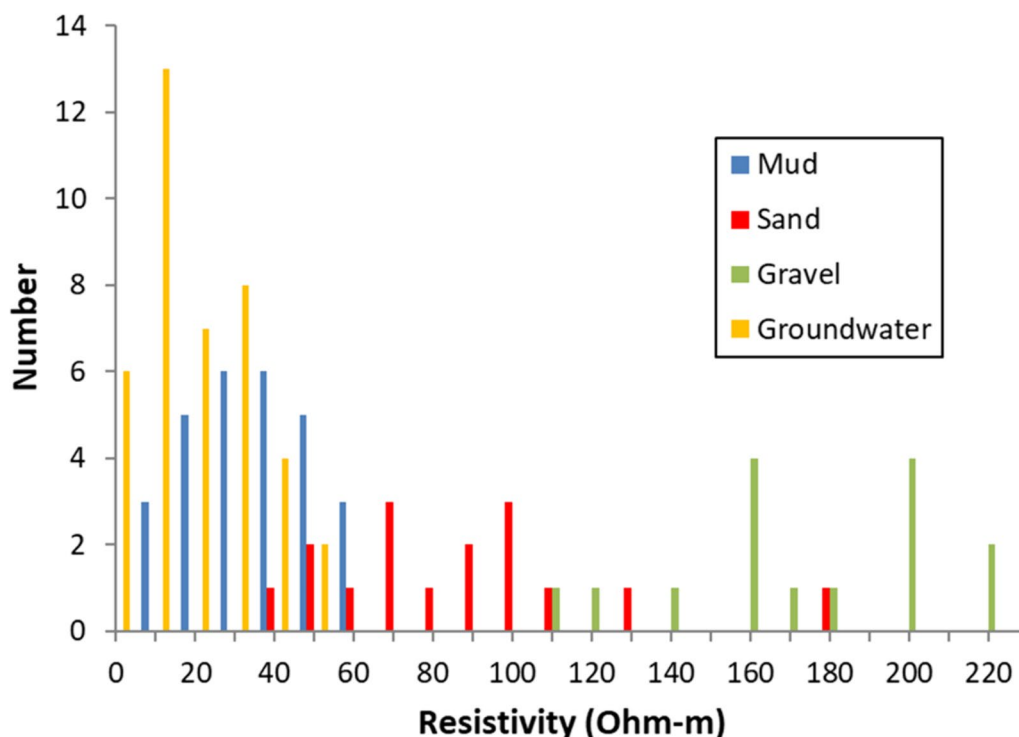
Fig. 3 The statistics for measured bulk resistivity of different sediment types from the borehole logging measurements and the groundwater resistivity

Chang *et al. Geoscience Letters*　　(2024) 11:25

Page 6 of 15

provided by the Geological Survey and Mining Management Agency (GSMMA 2001a, b). To develop a correlation between sediment types and formation factors (resistivity), we categorize the sediment types from the wellbore logs into only gravel, sand, and clay types. Figure 3 shows the statistics for the resistivity of different sediments. Archie (1942) suggested that the relationships between the in-situ resistivity of a saturated sedimentary rock to its porosity and pore-water resistivity can be described as follows:

$$\rho_b = a \cdot \rho_w \cdot \varnothing^{-m}, \tag{1}$$

where ρ_b is the bulk resistivity, a is the tortuosity factor, ρ_w is the pore-water resistivity, $\varnothing$ represents the porosity, and m represents the cementation exponent relative to the rock. In Eq. (1), the measured bulk resistivity is influenced by the resistivity of pore water. Thus, if the resistivities in the pore water vary widely, the bulk resistivity of the same sediment type can also vary significantly, irrespective of the sediment type. Conversely, when the resistivity of the groundwater is similar, the distribution of resistivities in sediment will display a consistent pattern that reflects various sediment types. Figure 3 shows the groundwater resistivity collected from the observation wells in Yilan plain. We may conclude from Fig. 3 that one can roughly differentiate gravel, sand from clay sediments based on their measured resistivity, since the groundwater resistivities are mainly focused within the range of 5 to 50 Ohm-m, similar to that of the mud sediments, and do not affect the classification analysis.

Geological model construction with machine learning

Supervised machine learning procedure

To transfer the resistivity model in Fig. 3 into the geology model, it is crucial to correlate the resistivity data with the sediment types. Without knowledge of the petrophysical relationships, one feasible way to transfer the resistivity model into the geology model is through machine learning approaches. Several steps are involved in interpreting the resistivity data using machine learning techniques, as depicted in Fig. 4.

Initially, a ground truth dataset is compiled for the Supervised Machine Learning (SML) process. This dataset comprises information extracted from records of 30 boreholes within the study area, encompassing data on both sediment type and resistivity logs. The sediment type serves as the target data (label), while the resistivity log acts as the feature data.

It is important to highlight that the resistivity values obtained from borehole data underwent multiple treatments before being employed to SML procedure. Firstly, a pre-processing step involved data inversion to obtain the true resistivity distribution from the apparent resistivity data. Secondly, a crucial labeling step was conducted, where the inverted resistivity values were resampled, digitized and labeled with their corresponding sediment types at 1-m interval. This procedure was facilitated by the resistivity log complemented with sediment type information from the borehole, enabling a direct correlation between resistivity values and sediment types. The labeling comprised three distinct
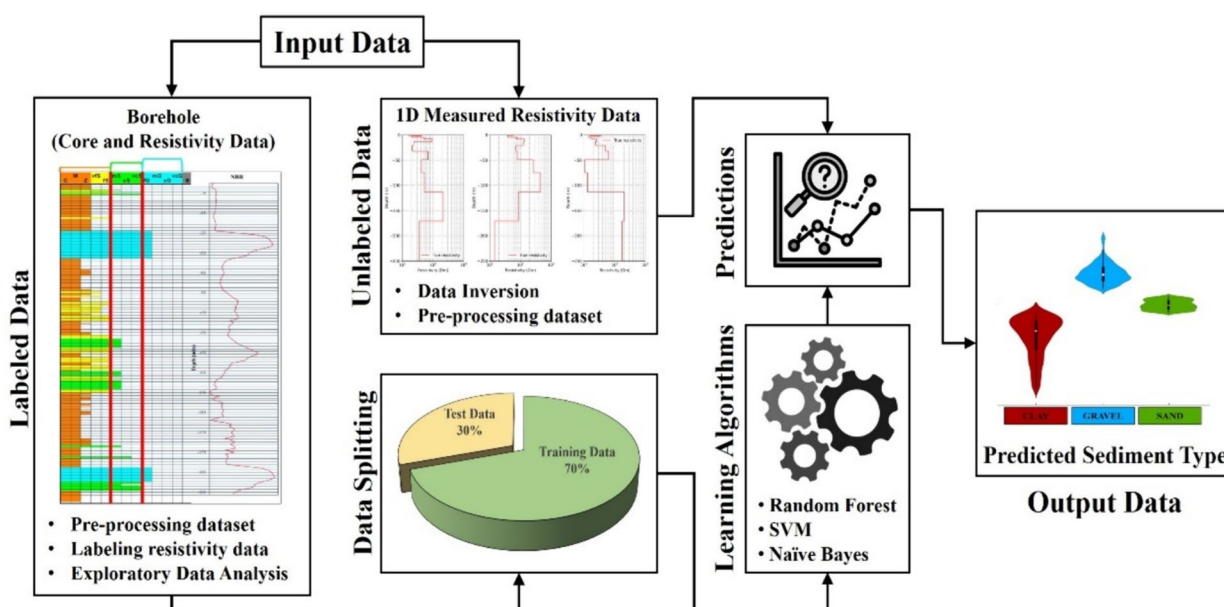
Fig. 4 A framework of the machine learning procedure to transfer resistivity model to apparent geological model

categories: Clay (C-fS), Sand (mS-vcS), and Gravel (fG-vcG). It is noteworthy that in this study, we combined clay (orange color) and very fine to fine sand (yellow color) into single category, as shown in Fig. 4. The final stage of borehole data preparation involved Exploratory Data Analysis (EDA) to delve deeper into the dataset, identifying any missing data or outliers.

Next, the borehole dataset was fed into three distinct SML algorithms, with the data partitioned into training and testing sets at a ratio of 70% for training and 30% for testing. These algorithms include Random Forest (Breiman 2001), Support Vector Machine (Lorena et al. 2011; Singh et al. 2016; Vapnik 1999), and Naive Bayes (H. Chen et al. 2021a, b; Lorena et al. 2011).

The performance of these models was subsequently evaluated to identify the most suitable algorithm for representing the dataset. Ultimately, predictions were made regarding the sediment type of the 1D measured resistivity data. It is imperative to note that this 1D data was resampled into 1-m interval using the Piecewise Cubic Hermite Interpolating Polynomial (PCHIP) (Rabbath & Corriveau 2019) before being utilized in the SML process, ensuring consistent intervals aligned with the borehole data.

Supervised machine learning evaluation.

We assessed the model performance and tuning parameters with cross-validation method, utilizing several indices, including accuracy, F1 score, precision, and recall. In this context, accuracy is the proportion of correctly classified examples, F1 score is a weighted harmonic mean of precision and recall, precision is the proportion of true positives among instances classified as positive, and recall is the proportion of true positives among all positive instances in the data.

Table 1 presents the evaluation of the three different SML approaches. Among these SML methods, Random Forest yielded the best classification performance, and therefore, we selected the classification criteria from Random Forest to transfer the resistivity model into the AGM. Figure 5 showcases the predicted sediment types of the borehole logs obtained through all three SML algorithms, alongside the actual sediment types obtained from the borehole record.

Furthermore, to enhance the clarity and interpretability of the SML results, we introduce the cross-sectional model (BB' profile) derived from the 3D resistivity model in this study (Fig. 6a), alongside the corresponding cross-sectional model derived from the AGM of the SML output (Fig. 6b), both at a depth of 100 m. The BB' profile is situated proximate to the AA' profile (*See* Fig. 1, 2) provided by GSMMA (2023), where the elevation gradually decreases from the western to the eastern area. The closest projected borehole location is denoted by the dashed black line. Upon comparison with the GSMMA's cross-section, our findings exhibit notable concordance, with the western region predominantly comprising gravel layers, while the eastern area is predominantly covered by mixed clay and sand layers.

Although our findings align with the previous study conducted by GSMMA, the vertical resolution (d_z) of our 3D modeling results has been reduced due to computational constraints. Initially, both the resistivity dataset from borehole logs and geoelectrical measurements were resampled into the same 1-m interval. However, for the 3D model, the vertical resolution has been adjusted to 2 m. This adjustment was necessary to accommodate the limitations of the available computing resources during the modeling process.

Despite this change, our model has notably enhanced the spatial resolution to 250 m in both horizontal directions (d_x, d_y). This improvement was achieved by incorporating additional geoelectrical measurements, resulting in a denser distribution of data points compared to utilizing borehole data alone to construct the model.

Results of the apparent geological model

Using the classification criteria built by correlating the lithology and resistivity with the machine-learning method, we can relate the regions with resistivity higher than 140 Ohm-m to the regions consisting mainly the gravels, the regions with resistivity between 60 and 140 Ohm-m to the sand sediments, and those with resistivity less than 60 Ohm-m to the sediments mainly composed of clays. Figure 7 shows the 3D resistivity model of the Yilan plain based on the resistivity measurements. In Fig. 7, the Isosurfaces of 140 Ohm-m and 60 Ohm-m were shown in the image to illustrate

Table 1 The supervised machine learning evaluation

Algorithm	Accuracy	F1	Precision	Recall	Resistivity boundary (Ωm)		
					Clay	Sand	Gravel
Random forest	0.91	0.90	0.90	0.91	0.01~60.60	60.64~140.01	140.18~1009.73
Support vector machine	0.88	0.87	0.84	0.90	0.01~60.48	60.53~141.55	141.67~1009.73
Naïve bayes	0.83	0.77	0.79	0.75	0.01~67.48	67.49~126.74	126.85~1009.73

Chang *et al. Geoscience Letters*   (2024) 11:25

Page 8 of 15
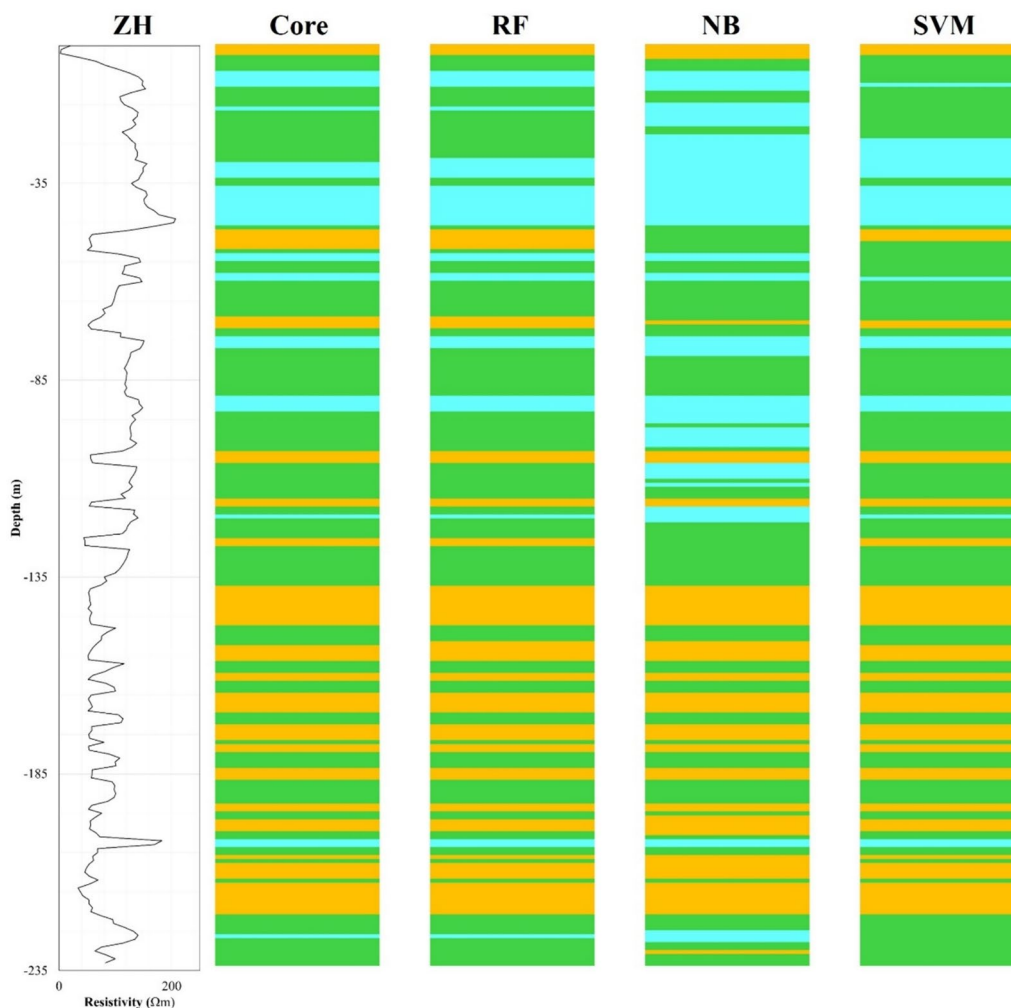
Fig. 5 The left panel displays the 1D resistivity log and core extracted from the borehole record, while the right panel shows the sediment types predcted by all three SML Algorithms. Clay is represented by orange, sand by green, and gravel by cyan

the resistivity variations in 3D sense. The regions with the resistivity higher than 140 Ohm-m are located at the upper fan and along the margin of the Yilan plain. And the yellow areas represent the regions having a resistivity between 60 and 140 Ohm-m. In Fig. 7, we transparent the conductive regions with resistivity less than 60 Ohm-m that should have blue and purple colors, in order to show the fluvial-delta sedimentary structures formed by mainly the sand and the gravels.

We further converted the 3D resistivity model into the clay-sand-gravel model based on the aforementioned criteria determined from machine learning. Figure 8a–j show the horizontal slices of sediment distribution at different depths in the Yilan Plain. Dating records from the borehole cores (GSMMA 2020) were also plotted in the figures to provide age references for the sediments. In general, the Carbon-14 dating ages decreased from about 8050–9,900 years before present

(yrBP) at 100-m deep to about 2,200–2,600 yrBP at a depth of 10-m deep. Furthermore, there are more Carbon-14 dating measurements collected in the sand area compared to the gravel and clay areas. Additionally, the dated ages roughly correspond to the depth for the measurements obtained in the sand area.

In Fig. 8, we observed several extruded gravel lobes associated with different river systems. For instance, there are two lobes in the southern part of the plain at a depth from 100 to 50 m. These two gravel lobes are associated with the Donshan and Lotung river systems. However, from 50 m to the surface, the gravel lobes associated with the Lanyang river and Lotung river became more distinct, while the gravel lobe of the Donshan river disappeared. These findings suggest that the Donshan river may have been more active than the Lotung and Lanyang rivers from 9,000–10,000 to about 5,000–5,500 yrBP. Yet the Lotung and Lanyang rivers became more active and
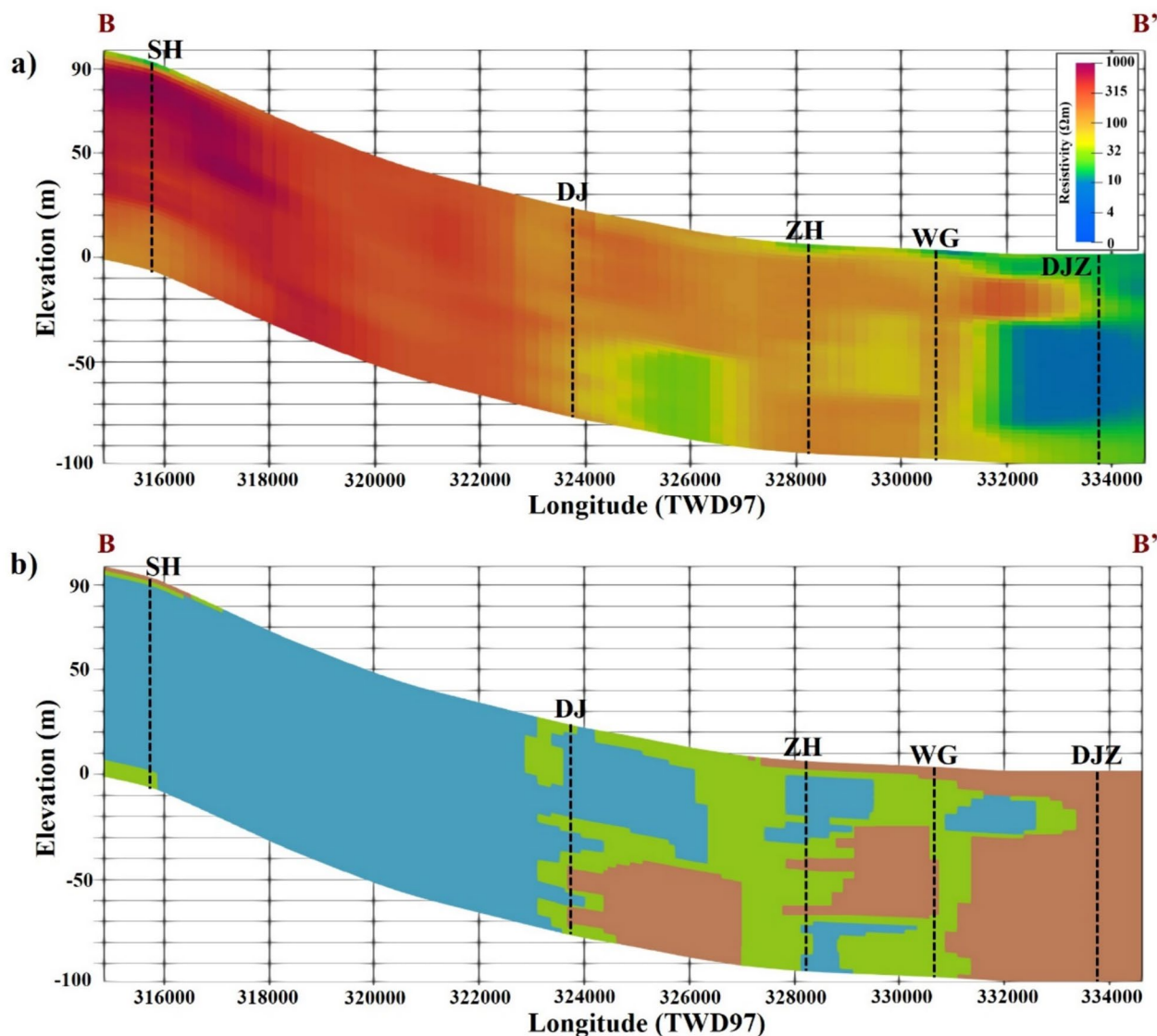
Fig. 6 a The cross-section of the resistivity model derived from the 3D model (BB' profile), and (**b**) the corresponding cross-section presenting the predicted sediment types obtained through the SML approach. The dashed-black line marking the nearest projected borehole sites of the AA' profile

dominated the fluvial system in the Yilan Plain after 5,800 yrBP.

Furthermore, the recently active Lanyang and Lotung rivers have caused the sand sediments to form a shape similar to the river mouth sandbar of the delta system after about 3,200 yrBP. The sandbar is oriented parallel to the modern coastline. The sedimentary facies determined from the sedimentary environment analysis (Su 2011) are roughly consistent with the distribution geometry of the sediments. Most of the environments in the boreholes remained quite stable and similar from about 10,000 yrBP to the present. However, at the Wujie (WG) observation well, the environment changes from shoreface to backshore at a depth of 60 m and turns into a meandering river at a depth of 20 m. In addition, the environment in Dajinzha (DJZ) changed from shoreface to backshore at a depth of 20 m. These findings also suggest that the the Lanyang and Lotung river systems gradually became the major fluvial systems in the Yilan Plain in the latest 5,000 yrBP to the present.

Chang *et al. Geoscience Letters*   (2024) 11:25

Page 10 of 15
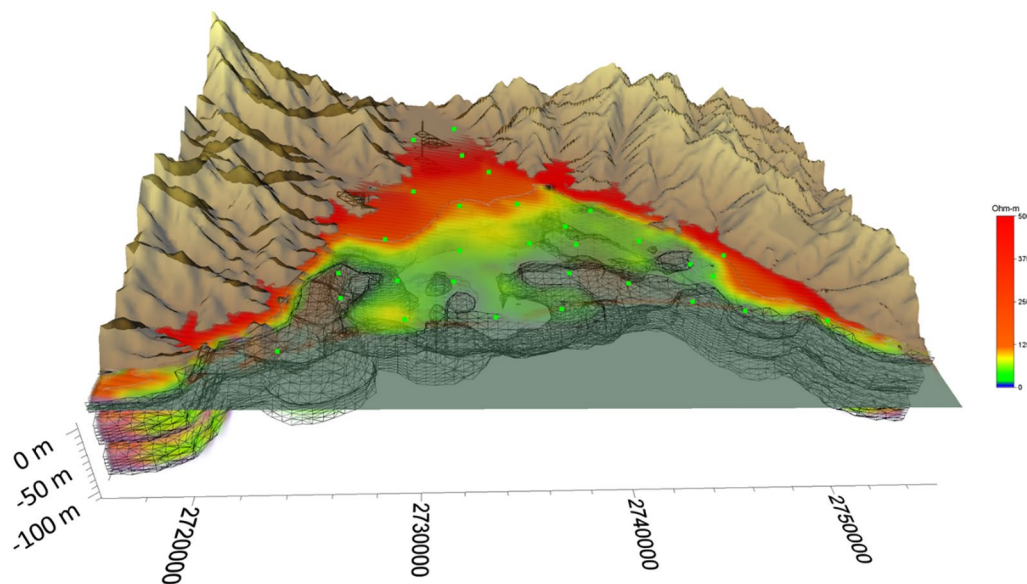
Fig. 7 The 3D resistivity model of the Yilan Plain. Green squares indicate the locations of observation wells. The isosurfaces indicate the resistivity distribution at 140 Ohm-m and 60 Ohm-m

Discussion

We can directly observe from Fig. 8a–j that the Yilan plain may be undergoing rapid subsidence, as evidenced by Carbon-14 dating of sediments in the shoreface environment at a depth of 100 m, which indicates an age of nearly 10,000 years Before Present (yrBP). There are three major factors that could influence changes in the morphologies of the Holocene coastal plain, including sea-level changes, sedimentation rates, and basin subsidence in the Yilan plain. In many low-lying areas worldwide, rapid sea-level rise during the early Holocene played a dominant role in shaping coastal environments (Amato et al. 2013; Stanley & Warne 1994). Following stabilization of sea levels during the mid- to late Holocene, sedimentation rates and neotectonics became the primary factors influencing coastal environment changes (Antonioli et al. 2009; Bird et al. 2010; Li et al. 2014). The interplay of these factors resulted in complex coastal morphologies in the Yilan plain. We used the reconstructed global sea level records from Hsieh et al. (2011) to account for the effects of sea-level changes. We specifically selected data from the same backshore face in the sand-dominated sediments to study subsidence due to neotectonics. In Hsieh et al. (2011), they assumed that the absolute sea-level curve around Taiwan matched the relative sea level obtained from the Sunda Shelf in Indonesia (Hanebuth et al. 2000), Singapore (Bird et al. 2007), and the Penghu Islands off western Taiwan (Y.-G. Chen & Liu 1996) for pre-11 ka, 6–9 ka, and 0–5 ka, respectively.

After correcting for mean sea level variations, we estimated the subsidence rate of the Yilan Basin, located at the tip of the Okinawa Trough, by assuming that the sedimentation rate of the same type of sediments from rivers in Yilan did not change drastically in the past 10,000 years. Figure 9(a) and Table 2 present Carbon-14 ages derived from sediments at various depths from wells located at Wusha (WS), Liming (LM), Zhunghsing (ZH), Beicheng (BC), and Shunan (SA). Additionally, in Fig. 9, we offer corrected depths, accounting for sea level changes, since the wells are situated at similar distances from the coast. After making these corrections and using data from the same sedimentary face, we estimated that the average subsidence rate in Yilan is approximately 8.5 mm/year (or 8.5 m/ka).

Additionally, we observed several sudden changes in the subsidence rate within the Carbon-14-age to depth curve. These abrupt subsidence events in the YYilan Plain occurred around 6000–7000 years before the present (yrBP) and 2000–3000 yrBP.

In addition, the dating ages and trends within the past 3000 years may suggest that the present is likely in a fast subsidence stage as well, as the youngest dating age of 120 yrBP is already at a depth of 5 m. Between these sudden subsidence periods, the average subsidence rate in the Yilan Plain was approximately 6.3 mm/year before 7000 yrBP, 10 mm/year between 6000 and 3000 yrBP, and 5 mm/year between 2000 and 120 yrBP. These subsidence rates are consistent with measurements of 5–10 mm/year
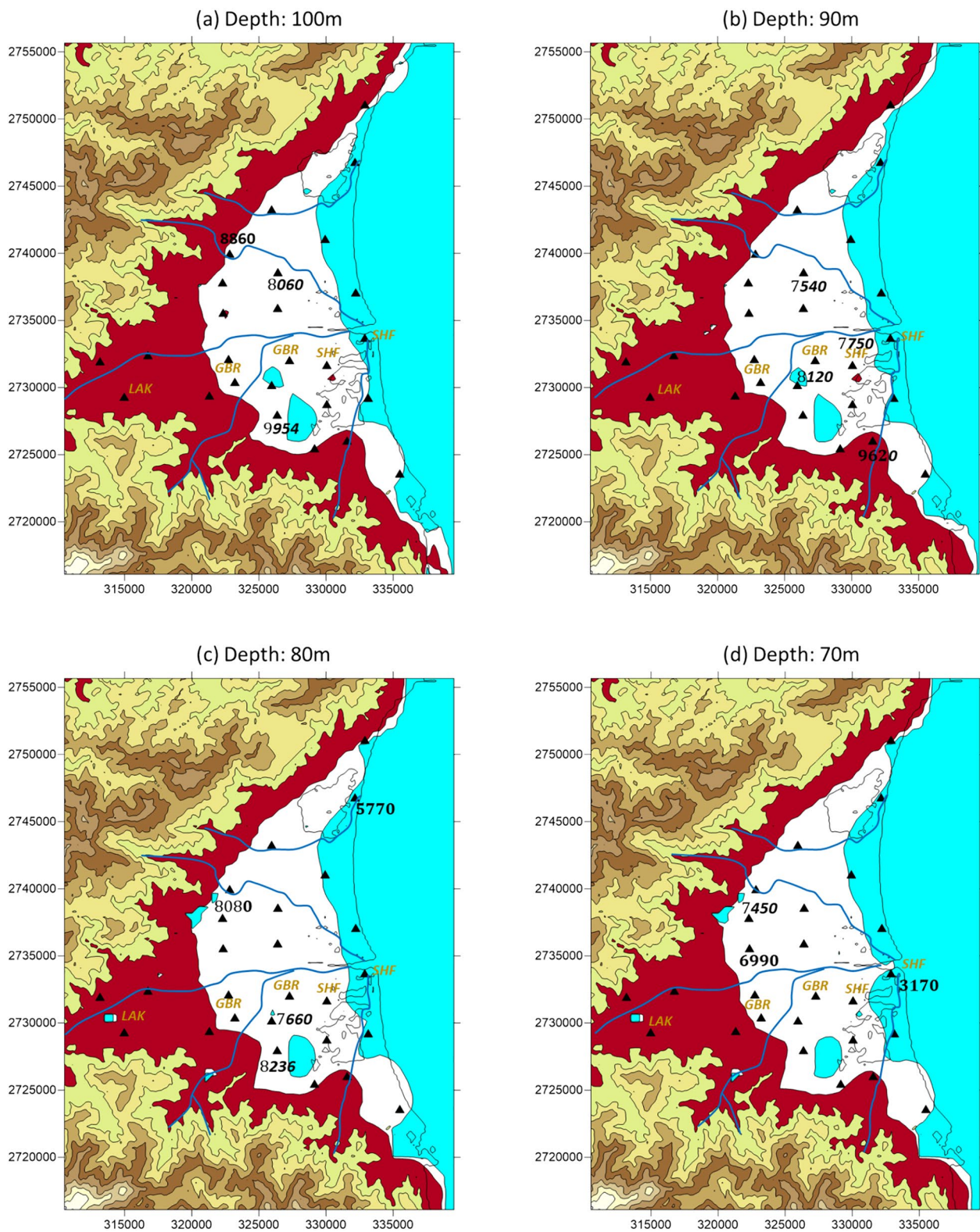
Fig. 8 Estimated Sediment Distribution Using Resistivity Measurements and Machine Learning in the Yilan Plain. The red color represents a gravel-dominated region, the white shows the region dominated by sand, and the blue color represents a clay-dominated region. Triangles indicate the locations of observation wells, with numbers representing C-14 dating ages. Brown characters indicate sedimentary facies along the AA' profile. Abbreviations: *GBR*—Gravelly Braided River, *SHF*—Shoreface, *BKS*—Backshore, *MDR*—Meandering River

Chang *et al. Geoscience Letters* (2024) 11:25

Page 12 of 15
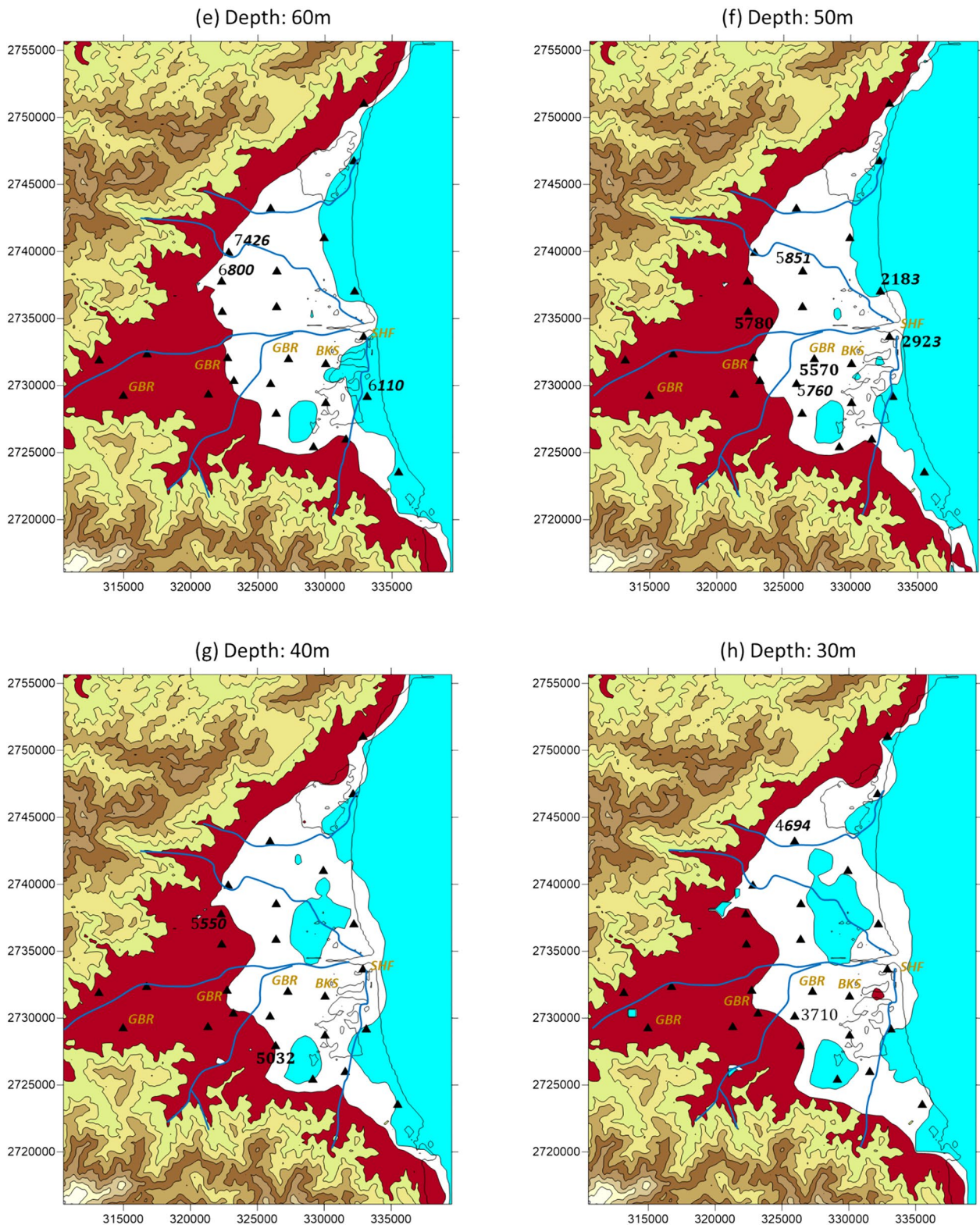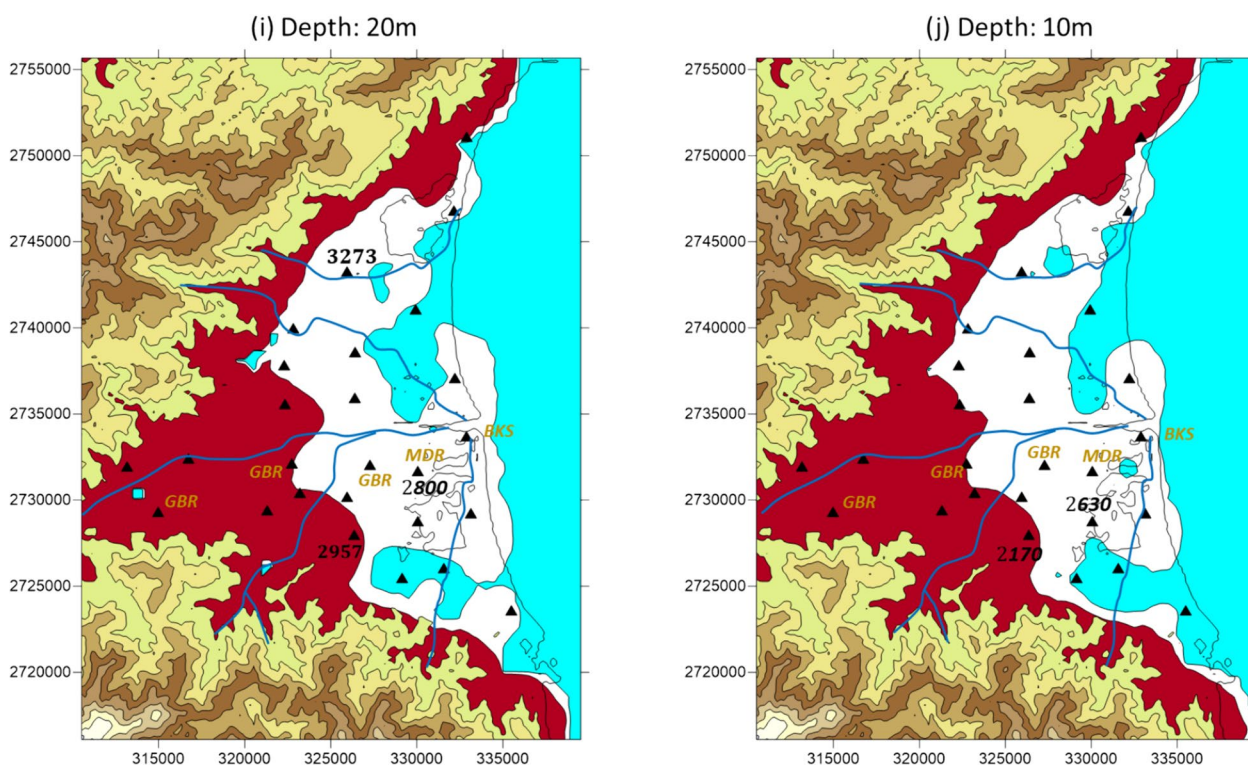
Fig. 8 continued

Fig. 8 continued
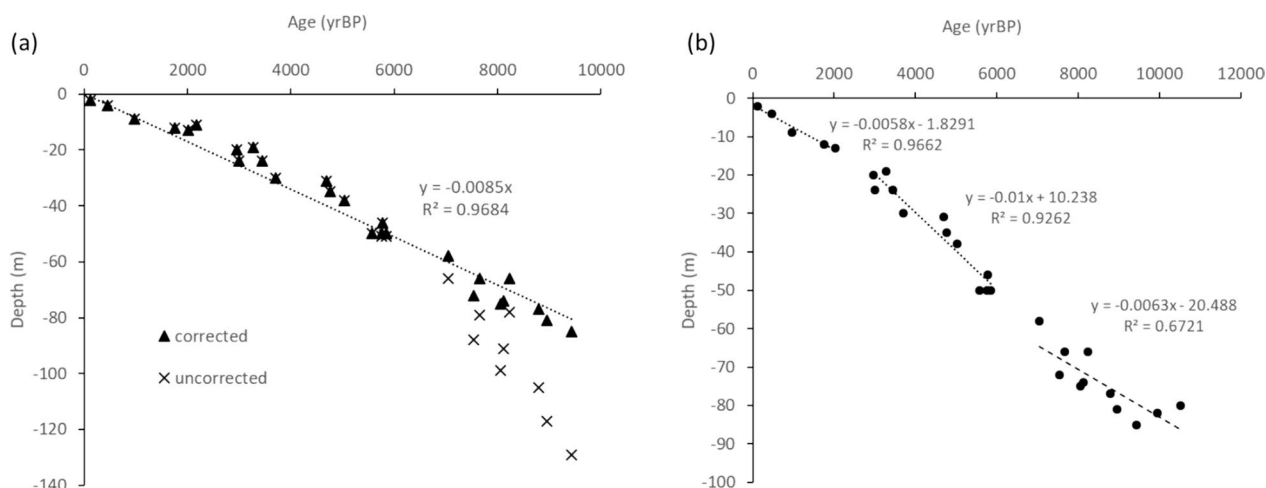
Fig. 9 a The Carbon-14 ages of sediments collected in the backshore sandy-dominated environment at various depths. Triangles represent data corrected for sea-level changes, while crosses represent uncorrected data. The dashed line illustrates the fitted trend for the corrected data. **b** The fitted trend showing the periods between sudden changes in the buried depth of the Carbon-14 ages-to-depth curve. Sudden subsidence may indicate seismic activity during these periods

obtained through GNSS observations (H.-Y. Chen et al. 2021a, b).

The sudden subsidence may be due to prehistoric earthquake events during active seismic periods. The findings also suggest a recurrence period of about 4000–5000 years for active seismic periods in Yilan. Compared with the Southern Okinawa Trough (SOT), our estimation for the subsidence rate of the Yilan Plain is about three to four times the average subsidence rate of the southernmost SOT (1.4–2.0 mm/yr) from 0.7 Ma to

Chang *et al. Geoscience Letters*   (2024) 11:25

Page 14 of 15

Table 2 The Carbon-14 dating ages and depths in the selected boreholes

Borehole	X	Y	Depth (m)	C-14 Ages (yrBP)
Zhunghsing (ZH)	328091	2731831	−24	3000±40
Zhunghsing (ZH)	328091	2731831	−50	5570±40
Zhunghsing (ZH)	328091	2731831	−129	9440±70
Beicheng (BC)	326777	2729989	−4	460±30
Beicheng (BC)	326777	2729989	−13	2020±30
Beicheng (BC)	326777	2729989	−30	3710±30
Beicheng (BC)	326777	2729989	−51	5760±30
Beicheng (BC)	326777	2729989	−66	7040±30
Beicheng (BC)	326777	2729989	−79	7660±30
Beicheng (BC)	326777	2729989	−91	8120±30
Beicheng (BC)	326777	2729989	−105	8790±30
Wusha (WS)	326773	2742142	−19	3273±50
Wusha (WS)	326773	2742142	−31	4694±54
Wusha (WS)	326773	2742142	−116	10510±60
Shunan (SA)	327157	2727748	−2.1	122±39
Shunan (SA)	327157	2727748	−9	969±41
Shunan (SA)	327157	2727748	−11	2170±40
Shunan (SA)	327157	2727748	−20	2957±42
Shunan (SA)	327157	2727748	−24	3450±40
Shunan (SA)	327157	2727748	−35	4760±40
Shunan (SA)	327157	2727748	−38	5032±51
Shunan (SA)	327157	2727748	−46	5780±40
Shunan (SA)	327157	2727748	−78	8236±86
Shunan (SA)	327157	2727748	−101	9954±87
Liming (LM)	327240	2738349	−12	1760±40
Liming (LM)	327240	2738349	−51	5851±48
Liming (LM)	327240	2738349	−88	7540±40
Liming (LM)	327240	2738349	−99	8060±40
Liming (LM)	327240	2738349	−117	8960±40

the present, as analyzed in the offshore data by Fang et al. (2020). These findings suggest that the plain at the tip of the SOT is still experiencing rapid subsidence, although the subsidence rate has decreased.

Conclusions

In this study, we attempt to reconstruct the intricate Holocene paleo-morphologies of the Yilan Plain with an innovative approach that combined resistivity measurements with machine learning techniques. The Yilan Plain, situated at the southwestern tip of the Okinawa Trough, held the key to understanding recent back-arc opening processes, making it an ideal subject of study. Our process involved interpolating inverted resistivity data to construct a 3D model, followed by developing classification criteria based on the relationship between resistivity values and registered sediment types in nearby boreholes using supervised machine learning. The culmination of this effort was the creation of a high-resolution Apparent Geological Model (AGM) that could be used to analyze the depositional environment in our study area and compare estimated sedimentary features with the environmental history.

Our classification criteria, based on lithology-resistivity correlations using the random forest machine-learning method, allowed us to categorize regions with resistivity values above 140 Ohm-m as predominantly gravel, those with resistivity between 60 and 140 Ohm-m as sand sediments, and regions with resistivity less than 60 Ohm-m as clay-dominated sediments. We then converted this 3D resistivity model into a clay-sand-gravel model based on the criteria. Our horizontal slices of sediment distribution at various depths in the Yilan Plain, complemented by borehole core dating records, provided crucial insights. Notably, the Carbon-14 dating ages in the sand sediments demonstrated greater consistency compared to gravel and clay areas. Additionally, we identified extruded gravel lobes associated with different river systems, shedding light on the historical activity patterns of these rivers.

Our findings also hinted at a phenomenon of rapid subsidence in the Yilan Plain. Through meticulous analysis and correction for sea-level changes, we estimated an average subsidence rate of approximately 8.5 mm/year. Intriguingly, we observed abrupt subsidence events at around 6000–7000 yrBP and 2000–3000 yrBP, accompanied by a sudden increase in depth of about 10 m during these periods. Between these episodes, the average subsidence rates varied, suggesting a possible link to prehistoric earthquake events during active seismic periods. Moreover, our results pointed to a recurrence period of approximately 4000–5000 years for active seismic periods in Yilan.

In conclusion, this study has uncovered a wealth of information about the Holocene paleo-morphologies of the Yilan Plain, leveraging innovative techniques and interdisciplinary approaches. Our integration of resistivity measurements, machine learning, and geological analysis has provided a deeper understanding of the region's geological history, sedimentary patterns, and seismic activity. These insights are not only valuable for advancing our knowledge of Yilan's past but also offer essential data for future environmental and geological studies in such dynamic regions.

Declarations

Competing interests
The authors declare that they have no competing interests.

Author details
[1]Department of Earth Sciences, National Central University, Jhong-li, Taoyuan, Taiwan. [2]Earthquake Disaster & Risk Evaluation and Management Center (E-DREaM), National Central University, Jhong-li, Taoyuan, Taiwan. [3]Center for Astronautical Physics and Engineering (CAPE), National Central University, Jhong-li, Taoyuan, Taiwan. [4]National Taiwan University, Taipei, Taiwan, ROC.

References
Amato V et al (2013) Relative sea level changes and paleogeographical evolution of the southern sele plain (Italy) during Holocene. Quatern Int 288:112–128

Antonioli F et al (2009) Holocene relative sea-level changes and vertical movements along the Italian and Istrian coastlines. Quatern Int 206(1):102–133

Archie GE (1942) The electrical resistivity log as an aid in determining some reservoir characteristics. Trans AIME 146(01):54–62. https://doi.org/10.2118/942054-G

Beresnev IA et al (2002) The use of multi-electrode resistivity imaging in gravel prospecting. J Appl Geophys 49(4):245–254. https://doi.org/10.1016/S0926-9851(02)00147-7

Bersezio R et al (2007) Combining sedimentological and geophysical data for high-resolution 3-D mapping of fluvial architectural elements in the quaternary Po plain (Italy). Sed Geol 202(1–2):230–248. https://doi.org/10.1016/j.sedgeo.2007.05.002

Bird MI et al (2007) An inflection in the rate of early mid-Holocene eustatic sea-level rise: a new sea-level curve from Singapore. Estuar Coast Shelf Sci 71(3):523–536. https://doi.org/10.1016/j.ecss.2006.07.004

Bird MI et al (2010) Punctuated eustatic sea-level rise in the early mid-Holocene. Geology 38(9):803–806

Breiman L (2001) Random Forests. Mach Learn 45:5–32

Chang PY et al (2020) An analysis of the subsurface fault systems with audio-magnetotelluric surveys in the western Ilan Plain of NE Taiwan. Terr Atmos Ocean Sci 31:551–564

Chen WS (2000) The study of sediments, depositional environments and stratigraphic correlations in the Lanyang Plain Central Geol. Survey Press, Taipei

Chen H-Y et al (2021a) A decade of global navigation satellite system/acoustic measurements of back-arc spreading in the southwestern Okinawa trough. Front Earth Sci 9:601138

Chen H et al (2021b) Improved naive Bayes classification algorithm for traffic risk management. EURASIP J Adv Signal Process 2021(1):1–12

Chen Y-G, Liu T-K (1996) Sea level changes in the last several thousand years, Penghu Islands. Taiwan Strait Quat Resea 45(3):254–262. https://doi.org/10.1006/qres.1996.0026

Chiang SC (1976) A seismic refraction prospecting of the Ilan plain. Mining Tech 14:215–221

Cockett R et al (2015) SimPEG: an open source framework for simulation and gradient based parameter estimation in geophysical applications. Comput Geosci 85:142–154

Fang P et al (2020) Neogene subsidence pattern in the multi-episodic extension systems: Insights from backstripping modelling of the Okinawa Trough. Mar Pet Geol 111:662–675. https://doi.org/10.1016/j.marpetgeo.2019.08.051

GSMMA. (2001). groundwater monitoring network in taiwan: the hydrogeology survey in the chianan plain and lanyang plain. Retrieved from Geological Survey and Mining Management Agency, Taipei.

GSMMA. (2001). groundwater monitoring network in taiwan: the hydro-geology survey in the chianan plain and lanyang plain. Retrieved from Central Geological Survey Taipei.

GSMMA. (2020). *Taiwan hydrogeological information database.* . Retrieved from Geological Survey and Mining Management Agency of Taiwan, Taipei.

GSMMA. (2023). Hydrogeological Database Combined Query Platform. Retrieved June 13, 2020, from Geological Survey and Mining Management Agency of Taiwan, Taipei. https://hydro.geologycloud.tw/map

Hanebuth T et al (2000) Rapid flooding of the Sunda shelf: a late-glacial sea-level record. Science 288(5468):1033–1035. https://doi.org/10.1126/science.288.5468.1033

Hsieh M-L et al (2011) Early holocene catastrophic mass-wasting event and fan-delta development on the Hua-tung coast, eastern Taiwan. Geomorphology 134(3):378–393. https://doi.org/10.1016/j.geomorph.2011.07.012

Hsu SK et al (1996) High-resolution detection of geologic boundaries from potential-field anomalies; an enhanced analytic signal technique. Geophysics 61(2):373

Lai KY et al (2009) The 2005 Ilan earthquake doublet and seismic crisis in Northeastern Taiwan: evidence for dyke intrusion associated with on-land propagation of the Okinawa Trough. Geophys J Int 179(2):678–686

Li G et al (2014) Sedimentary system response to the global sea level change in the East China Seas since the last glacial maximum. Earth Sci Rev 139:390–405. https://doi.org/10.1016/j.earscirev.2014.09.007

Lorena AC et al (2011) Comparing machine learning classifiers in potential distribution modelling. Expert Syst Appl 38(5):5268–5275

Pellicer XM, Gibson P (2011) Electrical resistivity and Ground Penetrating Radar for the characterisation of the internal architecture of Quaternary sediments in the Midlands of Ireland. J Appl Geophys 75(4):638–647. https://doi.org/10.1016/j.jappgeo.2011.09.019

Rabbath CA, Corriveau D (2019) A comparison of piecewise cubic Hermite interpolating polynomials, cubic splines and piecewise linear functions for the approximation of projectile aerodynamics. Def Technol 15(5):741–757. https://doi.org/10.1016/j.dt.2019.07.016

Rucker DF et al (2011) Electrical resistivity in support of geological mapping along the Panama Canal. Eng Geol 117(1–2):121–133

Sibuet JC et al (1998) Okinawa trough backarc basin: early tectonic and magmatic evolution. J Geophys Resea. https://doi.org/10.1029/98JB01823

Singh, A., et al. (2016). *A review of supervised machine learning algorithms.* Paper presented at the 2016 3rd International Conference on Computing for Sustainable Global Development (INDIACom).

Stanley DJ, Warne AG (1994) Worldwide initiation of Holocene marine deltas by deceleration of sea level rise. Science 265(5169):228–231

Su, C. C. (2011). The last interglacial depositional environment and tectonic characteristics of the Ilan Plain, northeastern Taiwan. (Master Master Thesis). National Taiwan University, Taipei, Taiwan.

Vapnik V (1999) The nature of statistical learning theory. Springer, New York

Publisher's Note